

## Engineering corner states by coupling two-dimensional topological insulators


Lizhou Liu,<sup>1,\*</sup> Jiaqi An<sup>2,\*</sup> Yafei Ren<sup>3</sup>, Ying-Tao Zhang,<sup>1,†</sup> Zhenhua Qiao<sup>2,4,‡</sup> and Qian Niu<sup>2</sup>

<sup>1</sup>College of Physics, Hebei Normal University, Shijiazhuang, Hebei 050024, China

<sup>2</sup>International Centre for Quantum Design of Functional Materials, CAS Key Laboratory of Strongly-Coupled Quantum Matter Physics, and Department of Physics, University of Science and Technology of China, Hefei, Anhui 230026, China

<sup>3</sup>Department of Physics, University of Delaware, Delaware 19716, USA

<sup>4</sup>Hefei National Laboratory, University of Science and Technology of China, Hefei 230088, China

 (Received 1 June 2024; revised 31 October 2024; accepted 19 December 2024; published 6 January 2025)

We theoretically find that the second-order topological insulator, i.e., corner states, can be engineered by coupling two copies of two-dimensional  $\mathbb{Z}_2$  topological insulators with opposite spin helicities. As concrete examples, we utilize Kane-Mele models (i.e., graphene with intrinsic spin-orbit coupling) to realize the corner states by setting the respective graphenes as  $\mathbb{Z}_2$  topological insulators with opposite intrinsic spin-orbit couplings. To exhibit its universality, we generalize our findings to other representative  $\mathbb{Z}_2$  topological insulators, e.g., the Bernevig-Hughes-Zhang model. An effective model is presented to reveal the physical origin of the corner states. We further show that the corner states can also be designed in other topological systems, e.g., by coupling quantum anomalous Hall systems with opposite Chern numbers. Our work suggests that interlayer coupling can be treated as a simple and efficient strategy to drive two-dimensional lower-order topological insulators to the higher-order ones.

DOI: [10.1103/PhysRevB.111.045403](https://doi.org/10.1103/PhysRevB.111.045403)

### I. INTRODUCTION

Topological insulators (TIs) represent a fascinating class of materials that exhibit insulating properties in their bulk while hosting topologically protected conducting states along their boundaries in two-dimensional (2D) systems or on their surfaces in three-dimensional (3D) systems [1–15]. Rich topological phases have been identified in the past decades. Particularly, in the presence of time-reversal symmetry, a  $\mathbb{Z}_2$  TI [16–25] has been proposed and realized, which is characterized by spin-helical edge states as represented by the pioneering Kane-Mele model [2,3] and Bernevig-Hughes-Zhang (BHZ) model [4] in 2D, which were later generalized to 3D [26,27]. In the absence of time-reversal symmetry, the quantum anomalous Hall effect (QAHE) with chiral-propagating edge modes has been widely studied in various model systems and materials candidates [11,28–51].

Recent advancements have generalized the topological phases to higher order [52–70]. In contrast to  $\mathbb{Z}_2$  TI or QAHE, the topologically protected states in the higher-order TIs are localized at the corners (0D states) in 2D systems or along hinges (1D states) in 3D systems [52,53]. The emergence of higher-order TIs introduces a new dimension to the topological classification of materials, offering the potential for novel electronic, photonic, and phononic applications [71–74]. By a case study in electronic systems, it was reported that 2D second-order TIs (SOTIs) can be realized in black phosphorene [75], twisted bilayer graphene at certain angles

[76], and graphyne [77–79] where the corner states are spin degenerate due to the time-reversal symmetry. Experimental observations of SOTI have so far been limited to hinge states in 3D bismuth [62]. However, the corner states in 2D higher-order materials lack experimental confirmation. Exploring a simple and effective scheme to design a 2D SOTI is necessary. Furthermore, a systematical strategy to generate SOTIs is to break the time-reversal symmetry of the  $\mathbb{Z}_2$  TIs by using an in-plane Zeeman field [80] where the states on one corner are not degenerate, which has later been applied to various material systems [81–87].

In this paper, we demonstrate that, without breaking the time-reversal symmetry, the SOTI in 2D spinful systems can be engineered by simply coupling two first-order topological insulators, e.g., by coupling two copies of  $\mathbb{Z}_2$  TIs as illustrated in Fig. 1(a). By using a model study, we first demonstrate the SOTI by coupling two  $\mathbb{Z}_2$  TIs using the Kane-Mele model by identifying the in-gap corner states. Then, we generalize our results to the SOTI induced by coupling two QAHEs with opposite Chern numbers. Below, we focus on the model systems on a honeycomb lattice, where  $\mathbb{Z}_2$  TI and QAHE can be realized by considering different ingredients [2,11]. The generalization to other seminal model systems (BHZ model) is provided in Ref. [88].

### II. SYSTEM HAMILTONIAN

The system Hamiltonian of the coupled two topological layers on the honeycomb lattice is shown below,

$$H = \begin{pmatrix} H_T & \eta \\ \eta^* & H_B \end{pmatrix}, \quad (1)$$

\*These authors contributed equally to this work.

†Contact author: zhangyt@mail.hebtu.edu.cn

‡Contact author: qiao@ustc.edu.cn

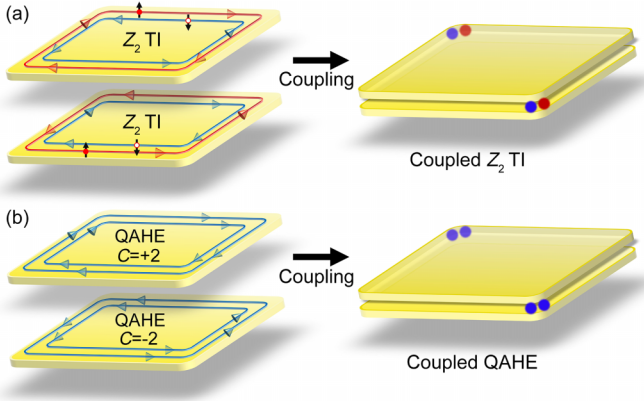


FIG. 1. Schematic plot of coupled topological insulators. (a) Left: Two decoupled  $\mathbb{Z}_2$  TI layers with opposite spin-helical edge states, i.e., spin-up edge modes in red respectively propagate clockwise and counterclockwise in the top and bottom layers, while spin-down edge modes in blue respectively propagate counterclockwise and clockwise in the top and bottom layers. Right: Coupling destroys all kinds of edge modes and gives rise to two Kramer pairs of corner states denoted by red and blue dots. (b) Left: Two decoupled QAHE layers with opposite Chern numbers, i.e., the edge modes propagate clockwise/counterclockwise in the top/bottom layer. Right: Coupling destroys all kinds of edge modes, and gives rise to four corner states denoted by blue dots.

where  $\eta$  measures the coupling strength between two separate layers,  $H_T$  and  $H_B$  are the modified Kane-Mele model Hamiltonians for the top and bottom graphene layers, respectively, which can be expressed as

$$H_\gamma = -t \sum_{(ij)} c_i^\dagger c_j + it_R \sum_{(ij)\alpha\beta} \hat{\mathbf{e}}_z \cdot (\boldsymbol{\sigma}_{\alpha\beta} \times \mathbf{d}_{ij}) c_{i\alpha}^\dagger c_{j\beta} + it_\gamma^\dagger \sum_{\langle\langle ij \rangle\rangle} v_{ij} c_i^\dagger s_z c_j + \lambda_\gamma \sum_{i\alpha} c_{i\alpha}^\dagger \sigma_z c_{i\alpha}, \quad (2)$$

where  $\gamma$  is  $T$  or  $B$  representing the top or bottom layer, and  $c_i^\dagger = (c_{i\uparrow}^\dagger, c_{i\downarrow}^\dagger)$  is the creation operator for an electron with spin up/down ( $\uparrow/\downarrow$ ) at the  $i$ th site. The first term is the nearest-neighbor hopping with an amplitude of  $t$ . The second term is the Rashba spin-orbit coupling with coupling strength  $t_R$ . The third term is the intrinsic spin-orbit coupling involving next-nearest-neighbor hopping with  $v_{ij} = \mathbf{d}_i \times \mathbf{d}_j / |\mathbf{d}_i \times \mathbf{d}_j|$  where  $\hat{\mathbf{d}}_{ij}$  is a unit vector pointing from site  $j$  to  $i$ , with coupling strength  $t_i$ . The last term corresponds to a uniform exchange field with a strength of  $\lambda$ . Without loss of generality, we only consider the AA-stacking case. Throughout this paper, we measure the Fermi level, intrinsic and Rashba spin-orbit couplings, and exchange energy in the unit of  $t$ .

### III. CORNER STATES IN COUPLED $\mathbb{Z}_2$ TIs

Let us begin with the seminal Kane-Mele model, as depicted in the left panel of Fig. 1(a), by setting  $t_R = \lambda_{T,B} = 0$ . In our consideration, we choose the zigzag graphene ribbon width to be  $N_y = 60a$ , with  $a$  being the lattice constant. We set the intrinsic spin-orbit couplings at the top and bottom graphene layers to be opposite, i.e.,  $t_1^T = -t_1^B = 0.1$ . When the two layers are isolated (i.e.,  $\eta = 0.0$ ), both exhibit the

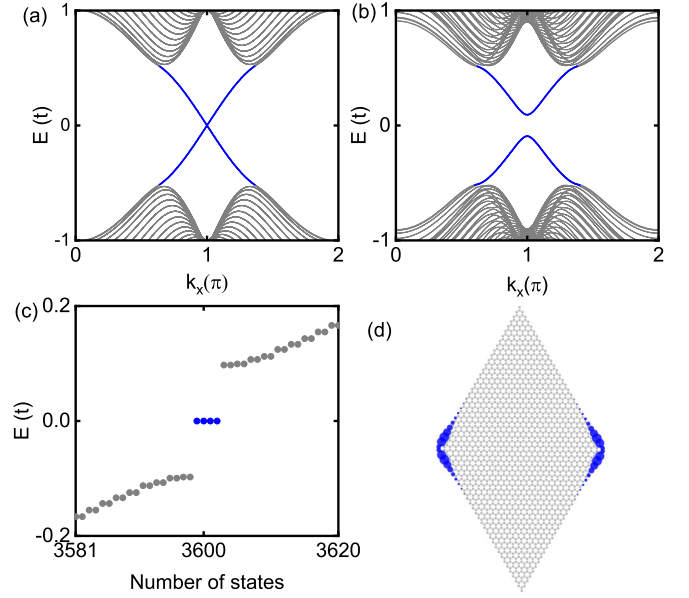


FIG. 2. (a), (b) Band structures of zigzag ribbons of decoupled and coupled  $\mathbb{Z}_2$  TIs with coupling strengths being (a)  $\eta = 0.0$  and (b)  $\eta = 0.2$ , respectively. Blue lines correspond to the spin-helical edge states. (c) Energy levels of diamond-shaped coupled graphene nanoflakes with the same parameters as those of (b). Blue dots correspond to in-gap corner states. (d) Probability distribution of the corner states. Other parameters are chosen to be  $t_1^T = -t_1^B = 0.1$ ,  $t_R = 0.0$ ,  $\lambda = 0.0$ ,  $N_y = 60a$  for the ribbon width, and the nanoflake size  $60a \times 60a$ .

well-known spin-helical edge modes, i.e., edge modes with opposite spins counterpropagate along the same boundary [see Fig. 2(a)]. The only difference is that, at the top and bottom layers, the same spin-polarized edge mode propagates clockwise and counterclockwise, respectively [see the left panel of Fig. 1(a)].

The stacking of two  $\mathbb{Z}_2$  TIs is topologically trivial as the gapless edge states from the same spin sector can couple and form an energy gap. As shown in Fig. 2(b), the edge states highlighted in blue become gapped when the interlayer coupling is turned on ( $\eta = 0.2$ ). A natural and general consequence is that the “+” TI phase plus the “-” TI phase gives nothing, i.e., a trivial insulator. Surprisingly, we show that although the first-order topological phase vanishes, the second-order topological phase arises.

To explore the second-order topology, an efficient approach is to explore the energy spectra of a fixed nanoflake, e.g., diamond-shaped nanoflake ( $60a \times 60a$ ) for graphene systems. As displayed in Fig. 2(c), there arise four zero-energy in-gap states (highlighted in blue dots) at the Fermi level. By analyzing the local density of states of the zero-energy states, one can see that these states are equally localized at the left and right corners, with each corner hosting a  $1/2$  electron charge. This directly indicates the formation of the SOTIs in 2D systems, which is robust to weak Rashba spin-orbit coupling [88]. Some other various representative nanoflakes are considered in Ref. [88]. We also successfully generalize these findings to other seminal  $\mathbb{Z}_2$  TIs, e.g., the BHZ model, as discussed in Ref. [88].

#### IV. PHYSICAL ORIGIN OF CORNER STATES

To understand the physical origin, let us first recall the effective Hamiltonian of the Kane-Mele model with an in-plane magnetic field [80] on the basis of  $\{\psi_\uparrow, \psi_\downarrow\}$ , which is written as [89]

$$h_0 = \begin{bmatrix} \mathbf{d}(\mathbf{k}) \cdot \sigma & B_x \\ B_x & -\mathbf{d}(-\mathbf{k}) \cdot \sigma \end{bmatrix}, \quad (3)$$

$$h_1 = \begin{bmatrix} \mathbf{d}_T(\mathbf{k}) \cdot \sigma & 0 & \eta & 0 \\ 0 & -\mathbf{d}_T(-\mathbf{k}) \cdot \sigma & 0 & \eta \\ \eta & 0 & \mathbf{d}_B(-\mathbf{k}) \cdot \sigma & 0 \\ 0 & \eta & 0 & -\mathbf{d}_B(\mathbf{k}) \cdot \sigma \end{bmatrix},$$

where  $T$  and  $B$  represent the top and bottom Kane-Mele system, respectively. Since the spin is a good quantum number in the Kane-Mele model without Rashba spin-orbit couplings, one can consider the single spin sectors separately, and the Hamiltonian on the basis of  $\{\psi_{T\uparrow}, \psi_{B\uparrow}\}$  can be written as

$$H = \begin{bmatrix} \mathbf{d}_T(\mathbf{k}) \cdot \sigma & \eta \\ \eta & \mathbf{d}_B(-\mathbf{k}) \cdot \sigma \end{bmatrix}. \quad (4)$$

Since  $t_1^T = -t_1^B$ , Eqs. (3) and (4) share the same form, except that the in-plane Zeeman field in Eq. (3) is replaced by the interlayer coupling in Eq. (4). In Eq. (4), the interlayer coupling couples the same spin-polarized but counterpropagating edge modes at different layers to open the edge gaps to form the corner states. It is highly noteworthy that in the coupled TI system the time-reversal symmetry is always preserved, i.e., the in-plane magnetization is not required.

To further analyze the physical origin of the corner states, we transform the Hamiltonian (1) to momentum space. The momentum-space Hamiltonian can be expressed as follows,

$$H(\mathbf{k}) = [f_x(\mathbf{k})\sigma_x + f_y(\mathbf{k})\sigma_y]s_0\tau_0 + f_1\sigma_z s_z \tau_z + \eta\sigma_0 s_0 \tau_x,$$

where

$$f_x(\mathbf{k}) = t[\cos ak_y + 2 \cos(ak_y/2) \cos(\sqrt{3}ak_x/2)],$$

$$f_y(\mathbf{k}) = t[\sin ak_y - 2 \sin(ak_y/2) \cos(\sqrt{3}ak_x/2)],$$

$$f_1(\mathbf{k}) = -2t_1^T [\sin \sqrt{3}ak_x - 2 \cos(3ak_y/2) \sin(\sqrt{3}ak_x/2)],$$

with  $\mathbf{k} = (k_x, k_y)$  being the quasimomentum,  $k_x$  ( $k_y$ ) is parallel to the zigzag (armchair) boundary direction, and  $a$  is the lattice constant. The  $t_R$  and  $\lambda_\gamma$  are set to 0 and are ignored.  $\sigma_i$ ,  $s_i$ , and  $\tau_i$  [ $i \in (0, x, y, z)$ ] are the Pauli matrices acting on the spin ( $\uparrow, \downarrow$ ), sublattice ( $A, B$ ), and interlayer degrees of freedom, respectively. Since spin is a good quantum number, we analyze the corner state origin from the spin-up sector:

$$H_\uparrow(\mathbf{k}) = [f_x(\mathbf{k})\sigma_x + f_y(\mathbf{k})\sigma_y]\tau_0 + f_1\sigma_z \tau_z + \eta\sigma_0 \tau_x.$$

When  $k_y = 0$ , the  $H_\uparrow(\mathbf{k})$  is invariant under the mirror-reflection symmetry of  $M_y = i\sigma_x \tau_x$ . Obviously, the  $M_y$  has two eigenvalues of  $\pm i$ . The eigenvectors of the  $+i$  subspace are  $\frac{\sqrt{2}}{2}[1, 0, 0, 1]^T$  and  $\frac{\sqrt{2}}{2}[0, 1, 1, 0]^T$ , whereas that for the  $-i$

where  $\mathbf{d}(\mathbf{k}) \cdot \sigma$  and  $-\mathbf{d}(-\mathbf{k}) \cdot \sigma$  represent the spin-up and spin-down sectors, respectively. In addition,  $\mathcal{T}\mathbf{d}(\mathbf{k}) \cdot \sigma \mathcal{T}^{-1} = -\mathbf{d}(-\mathbf{k}) \cdot \sigma$ , where the time-reversal operator  $\mathcal{T} = i s_y \mathcal{K}$ .  $B_x$  is the in-plane Zeeman field, which couples the spin-up and spin-down edge modes propagating along opposite directions, therefore inducing the edge gap to harbor the corner states.

In the present work, the same spin-polarized edge states propagate in opposite directions at different layers, with the effective Hamiltonian on the basis of  $\{\psi_{T\uparrow}, \psi_{T\downarrow}, \psi_{B\uparrow}, \psi_{B\downarrow}\}$  being written as

subspace are  $\frac{\sqrt{2}}{2}[0, 1, -1, 0]^T$  and  $\frac{\sqrt{2}}{2}[1, 0, 0, -1]^T$ . In these two subspaces,  $H_\uparrow(k_x, 0)$  can be separated into two decoupled parts,

$$H^\pm(k_x) = (\pm 1 + \eta \pm 2 \cos \sqrt{3}ak_x/2)\mu_x + 2t_1^T (\sin \sqrt{3}ak_x - 2 \sin \sqrt{3}ak_x/2)\mu_z, \quad (5)$$

where  $\pm$  indicates the subspace with  $\pm 1$  eigenvalue under  $M_y$ . We find that  $H^\pm(k_x)$  exhibit chiral symmetry, and  $\mu_x$  and  $\mu_z$  are Pauli matrices. The winding number  $v$  on the mirror symmetry axis  $M_y$  can be calculated by the following:

$$v = \frac{1}{2\pi} \int_{-\pi}^{\pi} \left( \mathbf{d}(k) \times \frac{d}{dk} \mathbf{d}(k) \right) dk_x. \quad (6)$$

We obtain the winding number  $v^\pm = \pm 1$ , which indicates the presence of second-order topological corner states in the system. The spin-down sector is the same as the spin-up, and the nonzero winding number ensures that corner states exist. Thus, there are four zero-energy corner states in the gap. The bulk band topology discussed above also shows the coexistence of topological crystal insulator phases, as discussed in Ref. [88], i.e., the presence of gapless edge states at the armchair boundaries.

#### V. CORNER STATES IN COUPLED QAHEs

Next, we show that the above strategy can also apply to QAHEs. In the following, we demonstrate the presence of SOTI by coupling two QAHE layers with opposite Chern numbers by setting  $t_1 = 0.0$ ,  $t_R = 0.2$ , and  $\lambda_T = -\lambda_B = 0.2$ . When the two layers are isolated (i.e.,  $\eta = 0.0$ ), the top and bottom graphene layers give rise to QAHEs with opposite Chern numbers of  $\mathcal{C} = \pm 2$ . As plotted in Fig. 3(a), the band structure of the zigzag ribbons exhibits doubly degenerate and chirally propagating gapless edge modes as shown in blue [clockwise and counterclockwise respectively at the top and bottom layers as depicted in Fig. 1(b)]. When the coupling is turned on with  $\eta = 0.1$ , the gapless edge modes become gapped as shown in Fig. 3(b). To confirm the presence of SOTI, we plot the energy spectra of the diamond-shaped nanoflakes as displayed in Fig. 3(c). Since we chose the

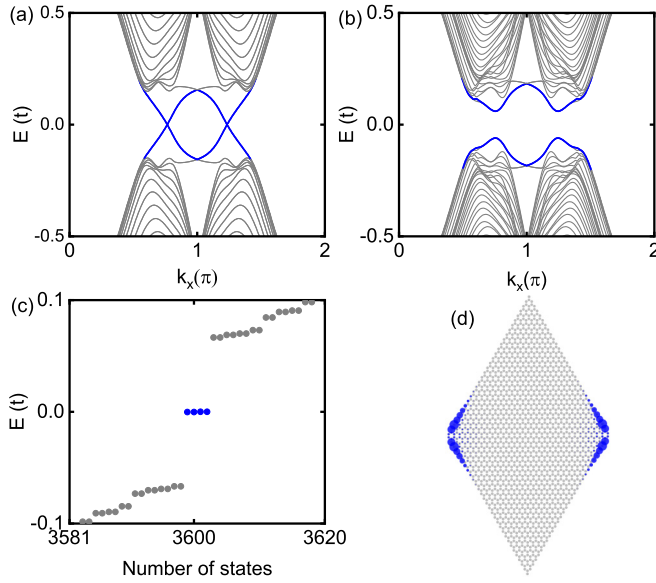


FIG. 3. (a), (b) Band structures of zigzag ribbons of decoupled and coupled QAHEs with coupling strengths being (a)  $\eta = 0.0$  and (b)  $\eta = 0.1$ , respectively. Blue lines denote the chiral edge states. (c) Energy levels of diamond-shaped coupled graphene nanoflakes, with the same parameters as those of (b). Blue dots correspond to in-gap corner states. (d) Probability distribution of the corner states. Other parameters are chosen to be  $t_l = 0.0$ ,  $t_R = 0.2$ ,  $\lambda_T = -\lambda_B = 0.2$ ,  $N_y = 60a$  for the ribbon width, and the nanoflake size  $60a \times 60a$ .

QAHE with  $C = \pm 2$  as the coupling unit, there are four in-gap corner states. Both the emergence of four zero-energy states and their wave-function distribution at the corners [see Fig. 3(d)] together strongly indicate the existence of SOTI. Similarly, this finding can also be generalized to other representative QAHE systems, e.g., the BHZ model with a Zeeman field [28,88], and the Dirac model [88].

## VI. TOPOLOGICAL PHASE DIAGRAMS

In the above discussions, we have chosen the specific case where the determining parameters are exactly opposite, i.e.,  $t_1^T = -t_1^B$  for coupled  $\mathbb{Z}_2$  TI or  $\lambda_T = -\lambda_B$  for coupled QAHE systems. Here, we systematically explore the influence of the relative signs on the topological phases. Figure 4(a) shows the topological phase diagram of coupled  $\mathbb{Z}_2$  TIs in the parameter spaces of  $(t_1^T, t_1^B)$ . One can see that there are four regions, which respectively belong to SOTI phases and weak TI phases. One can see that as long as the signs of  $t_1^T$  and  $t_1^B$  are different, any coupling can lead to the formation of SOTI (see the second and fourth quadrants), and the in-gap corner state remains at zero energy. But, when the signs of  $t_1^T$  and  $t_1^B$  are identical, the coupling can result in either weak TI or SOTI. A similar phase diagram as plotted in Fig. 4(b) is obtained for the coupled QAHE systems. For example, when  $\lambda_T$  and  $\lambda_B$  have different signs, the system is driven into SOTI, but when they have identical signs, it can induce either SOTI or QAHE with  $C = \pm 4$ .

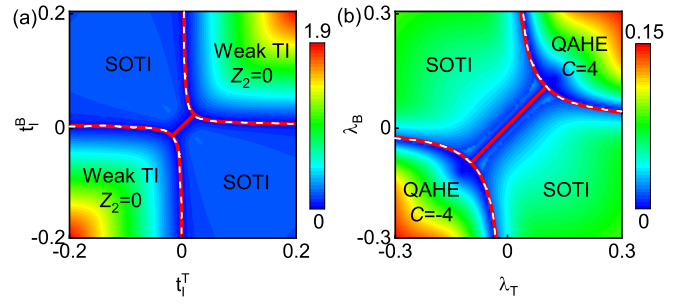


FIG. 4. (a) Phase diagram as functions of the intrinsic spin-orbit couplings  $t_1^T$  and  $t_1^B$  for the coupled  $\mathbb{Z}_2$  TIs. Other parameters are set to be  $t_R = 0.0$ ,  $\lambda = 0.0$ , and  $\eta = 0.2$ . (b) Phase diagram as functions of the exchange fields  $\lambda_T$  and  $\lambda_B$  for the coupled QAHEs. Other parameters are set to be  $t_R = 0.2$ ,  $t_l = 0.0$ , and  $\eta = 0.1$ . Dotted lines are the phase boundaries. Here, the bulk gap is used for the TI, weak TI, and QAHE regions, while the edge gap is used for the SOTI region.

To clearly understand and determine the phase boundaries, we employ the low-energy continuum model expanded at valley  $K/K'$ ,

$$H_{\text{eff}} = \begin{bmatrix} H_{\text{eff}}^T & \eta\sigma_0s_0 \\ \eta\sigma_0s_0 & H_{\text{eff}}^B \end{bmatrix}, \quad (7)$$

where

$$H_{\text{eff}}^{T,B} = 3t/2(\sigma_xk_x + \sigma_yk_y)\mathbf{1}_s + 3t_R/2(\sigma_xs_y - \sigma_ys_x) + 3\sqrt{3}t_1^{T,B}\sigma_zs_z + \lambda_{T,B}s_z\mathbf{1}_\sigma. \quad (8)$$

For the weak TI and SOTI phase boundaries, we set  $t_R = 0$ ,  $\lambda_{T,B} = 0$ , and impose the bulk gap closing condition of  $\varepsilon = 0$ . One can obtain the topological phase transition boundary satisfying

$$t_1^T t_1^B = \eta^2/27, \quad (9)$$

which shows perfect consistency with the direct band-structure calculation. Similarly, for the QAHE and SOTI phase boundaries, by setting  $t_l = 0$ , the topological phase transition boundary satisfies

$$\lambda_T \lambda_B = \eta^2, \quad (10)$$

which also agrees well with the direct band-structure calculation from the tight-binding model.

## VII. CONCLUSIONS

We have shown that the SOTIs in spinful systems can be engineered without breaking the time-reversal symmetry, by simply introducing an interlayer coupling in two  $\mathbb{Z}_2$  TIs with opposite spin helicities within the framework of the Kane-Mele model. A minimal model was presented to help understand the formation of SOTIs, i.e., the interaction between the counterpropagating edge modes with the same spin at different layers opens the edge gap. The nonzero

winding number in the high-symmetry line direction protects the existence of corner states. Inspired by these findings, we have also found that coupling two QAHEs with opposite Chern numbers can also lead to the formation of SOTIs, by using the graphene model with the Rashba effect. The generalization of these findings to the BHZ model suggests the universal characteristic of our proposed strategy of engineering SOTIs by coupling any kind of 2D topological systems.

## ACKNOWLEDGMENTS

This work was financially supported by the National Natural Science Foundation of China (Grants No. 12074097, No. 11974327, and No. 12004369), Natural Science Foundation of Hebei Province (Grant No. A2024205025), Anhui Initiative in Quantum Information Technologies (Grant No. AHY170000), and Innovation Program for Quantum Science and Technology (Grant No. 2021ZD0302800). The supercomputing service of USTC is gratefully acknowledged.

- [1] F. D. M. Haldane, Model for a quantum Hall effect without Landau levels: Condensed-matter realization of the “parity anomaly”, *Phys. Rev. Lett.* **61**, 2015 (1988).
- [2] C. L. Kane and E. J. Mele,  $Z_2$  topological order and the quantum spin Hall effect, *Phys. Rev. Lett.* **95**, 146802 (2005).
- [3] C. L. Kane and E. J. Mele, Quantum spin Hall effect in graphene, *Phys. Rev. Lett.* **95**, 226801 (2005).
- [4] B. A. Bernevig, T. L. Hughes, and S.-C. Zhang, Quantum spin Hall effect and topological phase transition in HgTe quantum wells, *Science* **314**, 1757 (2006).
- [5] J. E. Moore, The birth of topological insulators, *Nature (London)* **464**, 194 (2010).
- [6] Y. Ando, Topological insulator materials, *J. Phys. Soc. Jpn.* **82**, 102001 (2013).
- [7] R. S. K. Mong, A. M. Essin, and J. E. Moore, Antiferromagnetic topological insulators, *Phys. Rev. B* **81**, 245209 (2010).
- [8] F. Liu, Two-dimensional topological insulators: past, present and future, *Coshare Sci.* **01**, 03 (2023).
- [9] X.-L. Qi and S.-C. Zhang, Topological insulators and superconductors, *Rev. Mod. Phys.* **83**, 1057 (2011).
- [10] Z. Qiao, W.-K. Tse, H. Jiang, Y. G. Yao, and Q. Niu, Two-dimensional topological insulator state and topological phase transition in bilayer graphene, *Phys. Rev. Lett.* **107**, 256801 (2011).
- [11] Z. Qiao, S. A. Yang, W. Feng, W. K. Tse, J. Ding, Y. Yao, J. Wang, and Q. Niu, Quantum anomalous Hall effect in graphene from Rashba and exchange effects, *Phys. Rev. B* **82**, 161414(R) (2010).
- [12] M. Z. Hasan and C. L. Kane, Colloquium: Topological insulators, *Rev. Mod. Phys.* **82**, 3045 (2010).
- [13] A. Bansil, H. Lin, and T. Das, Colloquium: Topological band theory, *Rev. Mod. Phys.* **88**, 021004 (2016).
- [14] Y. Ren, Z. Qiao, and Q. Niu, Topological phases in two-dimensional materials: a review, *Rep. Prog. Phys.* **79**, 066501 (2016).
- [15] S. Q. Shen, Half quantized Hall effect, *Coshare Sci.* **02**, 01 (2024).
- [16] T. Olsen, E. Andersen, T. Okugawa, D. Torelli, T. Deilmann, and K. S. Thygesen, Discovering two-dimensional topological insulators from high-throughput computations, *Phys. Rev. Mater.* **3**, 024005 (2019).
- [17] A. Marrazzo, M. Gibertini, D. Campi, N. Mounet, and N. Marzari, Relative abundance of  $Z_2$  topological order in exfoliable two-dimensional insulators, *Nano Lett.* **19**, 8431 (2019).
- [18] K. Choudhary, K. F. Garrity, J. Jiang, R. Pachter, and F. Tavazza, Computational search for magnetic and non-magnetic 2D topological materials using unified spin-orbit spillage screening, *npj Comput. Mater.* **6**, 49 (2020).
- [19] R.-J. Slager, A. Mesaros, V. Juričić, and J. Zaanen, The space group classification of topological band-insulators, *Nat. Phys.* **9**, 98 (2013).
- [20] J. Kruthoff, J. de Boer, J. van Wezel, C. L. Kane, and R.-J. Slager, Topological classification of crystalline insulators through band structure combinatorics, *Phys. Rev. X* **7**, 041069 (2017).
- [21] B. Bradlyn, L. Elcoro, J. Cano, M. G. Vergniory, Z. Wang, C. Felser, M. I. Aroyo, and B. A. Bernevig, Topological quantum chemistry, *Nature (London)* **547**, 298 (2017).
- [22] H. C. Po, A. Vishwanath, and H. Watanabe, Symmetry-based indicators of band topology in the 230 space groups, *Nat. Commun.* **8**, 50 (2017).
- [23] T. Zhang, Y. Jiang, Z. Song, H. Huang, Y. He, Z. Fang, H. Weng, and C. Fang, Catalogue of topological electronic materials, *Nature (London)* **566**, 475 (2019).
- [24] M. G. Vergniory, L. Elcoro, C. Felser, N. Regnault, B. A. Bernevig, and Z. Wang, A complete catalogue of high-quality topological materials, *Nature (London)* **566**, 480 (2019).
- [25] F. Tang, H. C. Po, A. Vishwanath, and X. Wan, Comprehensive search for topological materials using symmetry indicators, *Nature (London)* **566**, 486 (2019).
- [26] L. Fu, C. L. Kane, and E. J. Mele, Topological insulators in three dimensions, *Phys. Rev. Lett.* **98**, 106803 (2007).
- [27] R. Roy, Topological phases and the quantum spin Hall effect in three dimensions, *Phys. Rev. B* **79**, 195322 (2009).
- [28] C.-X. Liu, X.-L. Qi, X. Dai, Z. Fang, and S.-C. Zhang, Quantum anomalous Hall effect in  $Hg_{1-y}Mn_yTe$  quantum wells, *Phys. Rev. Lett.* **101**, 146802 (2008).
- [29] N. Nagaosa, J. Sinova, S. Onoda, A. H. MacDonald, and N. P. Ong, Anomalous Hall effect, *Rev. Mod. Phys.* **82**, 1539 (2010).
- [30] H. Weng, R. Yu, X. Hu, X. Dai, and Z. Fang, Quantum anomalous Hall effect and related topological electronic states, *Adv. Phys.* **64**, 227 (2015).
- [31] G. Xu, H. Weng, Z. Wang, X. Dai, and Z. Fang, Chern semimetal and the quantized anomalous Hall effect in  $HgCr_2Se_4$ , *Phys. Rev. Lett.* **107**, 186806 (2011).
- [32] C.-X. Liu, S.-C. Zhang, and X.-L. Qi, The quantum anomalous Hall effect: Theory and experiment, *Annu. Rev. Condens. Matter Phys.* **7**, 301 (2016).
- [33] K. He, Y. Wang, and Q.-K. Xue, Topological materials: Quantum anomalous Hall system, *Annu. Rev. Condens. Matter Phys.* **9**, 329 (2018).
- [34] C.-Z. Chang, C.-X. Liu, and A. H. MacDonald, Colloquium: Quantum anomalous Hall effect, *Rev. Mod. Phys.* **95**, 011002 (2023).

- [35] R. Mei, Y.-F. Zhao, C. Wang, Y. Ren, D. Xiao, C.-Z. Chang, and C.-X. Liu, Electrically controlled anomalous Hall effect and orbital magnetization in topological magnet  $\text{MnBi}_2\text{Te}_4$ , *Phys. Rev. Lett.* **132**, 066604 (2024).
- [36] R. Yu, W. Zhang, H.-J. Zhang, S.-C. Zhang, X. Dai, and Z. Fang, Quantized anomalous Hall effect in magnetic topological insulators, *Science* **329**, 61 (2010).
- [37] S.-C. Wu, G. Shan, and B. Yan, Prediction of near-room-temperature quantum anomalous Hall effect on honeycomb materials, *Phys. Rev. Lett.* **113**, 256401 (2014).
- [38] C. Fang, M. J. Gilbert, and B. A. Bernevig, Large-Chern-number quantum anomalous Hall effect in thin-film topological crystalline insulators, *Phys. Rev. Lett.* **112**, 046801 (2014).
- [39] Z. Qiao, W. Ren, H. Chen, L. Bellaiche, Z. Zhang, A. H. MacDonald, and Q. Niu, Quantum anomalous Hall effect in graphene proximity coupled to an antiferromagnetic insulator, *Phys. Rev. Lett.* **112**, 116404 (2014).
- [40] Q.-Z. Wang, X. Liu, H.-J. Zhang, N. Samarth, S.-C. Zhang, and C.-X. Liu, Quantum anomalous Hall effect in magnetically doped  $\text{InAs}/\text{GaSb}$  quantum wells, *Phys. Rev. Lett.* **113**, 147201 (2014).
- [41] G. Xu, B. Lian, and S.-C. Zhang, Intrinsic quantum anomalous Hall effect in the kagome lattice  $\text{Cs}_2\text{LiMn}_3\text{F}_{12}$ , *Phys. Rev. Lett.* **115**, 186802 (2015).
- [42] H. Sun, B. Xia, Z. Chen, Y. Zhang, P. Liu, Q. Yao, H. Tang, Y. Zhao, H. Xu, and Q. Liu, Rational design principles of the quantum anomalous Hall effect in superlatticelike magnetic topological insulators, *Phys. Rev. Lett.* **123**, 096401 (2019).
- [43] Z. F. Wang, Z. Liu, and F. Liu, Quantum anomalous Hall effect in 2D organic topological insulators, *Phys. Rev. Lett.* **110**, 196801 (2013).
- [44] S. Qi, Z. Qiao, X. Deng, E. D. Cubuk, H. Chen, W. Zhu, E. Kaxiras, S. B. Zhang, X. Xu, and Z. Zhang, High-temperature quantum anomalous Hall effect in  $n$ - $p$  codoped topological insulators, *Phys. Rev. Lett.* **117**, 056804 (2016).
- [45] P. Högl, T. Frank, K. Zollner, D. Kochan, M. Gmitra, and J. Fabian, Quantum anomalous Hall effects in graphene from proximity-induced uniform and staggered spin-orbit and exchange coupling, *Phys. Rev. Lett.* **124**, 136403 (2020).
- [46] T. Devakul and L. Fu, Quantum anomalous Hall effect from inverted charge transfer gap, *Phys. Rev. X* **12**, 021031 (2022).
- [47] C.-Z. Chang, J. Zhang, X. Feng, J. Shen, Z. Zhang, M. Guo, K. Li, Y. Ou, P. Wei, L.-L. Wang, Z.-Q. Ji, Y. Feng, S. Ji, X. Chen, J. Jia, X. Dai, Z. Fang, S.-C. Zhang, K. He, Y. Wang *et al.*, Experimental observation of the quantum anomalous Hall effect in a magnetic topological insulator, *Science* **340**, 167 (2013).
- [48] C.-Z. Chang, W. Zhao, D. Y. Kim, P. Wei, J. K. Jain, C. Liu, M. H. W. Chan, and J. S. Moodera, Zero-field dissipationless chiral edge transport and the nature of dissipation in the quantum anomalous Hall state, *Phys. Rev. Lett.* **115**, 057206 (2015).
- [49] C.-Z. Chang, W. Zhao, D. Y. Kim, H. Zhang, B. A. Assaf, D. Heiman, S.-C. Zhang, C. Liu, M. H. W. Chan, and J. S. Moodera, High-precision realization of robust quantum anomalous Hall state in a hard ferromagnetic topological insulator, *Nat. Mater.* **14**, 473 (2015).
- [50] Y. Deng, Y. Yu, M. Z. Shi, Z. Guo, Z. Xu, J. Wang, X. H. Chen, and Y. Zhang, Quantum anomalous Hall effect in intrinsic magnetic topological insulator  $\text{MnBi}_2\text{Te}_4$ , *Science* **367**, 895 (2020).
- [51] M. Serlin, C. L. Tschirhart, H. Polshyn, Y. Zhang, J. Zhu, K. Watanabe, T. Taniguchi, L. Balents, and A. F. Young, Intrinsic quantized anomalous Hall effect in a moiré heterostructure, *Science* **367**, 900 (2020).
- [52] W. A. Benalcazar, B. A. Bernevig, and T. L. Hughes, Quantized electric multipole insulators, *Science* **357**, 61 (2017).
- [53] W. A. Benalcazar, B. A. Bernevig, and T. L. Hughes, Electric multipole moments, topological multipole moment pumping, and chiral hinge states in crystalline insulators, *Phys. Rev. B* **96**, 245115 (2017).
- [54] T. Li, P. Zhu, W. A. Benalcazar, and T. L. Hughes, Fractional disclination charge in two-dimensional  $C_n$ -symmetric topological crystalline insulators, *Phys. Rev. B* **101**, 115115 (2020).
- [55] G. van Miert and C. Ortix, Higher-order topological insulators protected by inversion and rotoinversion symmetries, *Phys. Rev. B* **98**, 081110(R) (2018).
- [56] W. A. Benalcazar, T. Li, and T. L. Hughes, Quantization of fractional corner charge in  $C_n$ -symmetric higher-order topological crystalline insulators, *Phys. Rev. B* **99**, 245151 (2019).
- [57] F. Schindler, M. Brzezinska, W. A. Benalcazar, M. Iraola, A. Bouhon, S. S. Tsirkin, M. G. Vergniory, and T. Neupert, Fractional corner charges in spin-orbit coupled crystals, *Phys. Rev. Res.* **1**, 033074 (2019).
- [58] Z. Song, Z. Fang, and C. Fang,  $(d - 2)$ -dimensional edge states of rotation symmetry protected topological states, *Phys. Rev. Lett.* **119**, 246402 (2017).
- [59] F. Schindler, A. M. Cook, M. G. Vergniory, Z. Wang, S. S. P. Parkin, B. A. Bernevig, and T. Neupert, Higher-order topological insulators, *Sci. Adv.* **4**, eaat0346 (2018).
- [60] J. Langbehn, Y. Peng, L. Trifunovic, F. von Oppen, and P. W. Brouwer, Reflection-symmetric second-order topological insulators and superconductors, *Phys. Rev. Lett.* **119**, 246401 (2017).
- [61] C.-H. Hsu, X. Zhou, T.-R. Chang, Q. Ma, N. Gedik, A. Bansil, S.-Y. Xu, H. Lin, and L. Fu, Topology on a new facet of bismuth, *Proc. Natl. Acad. Sci. USA* **116**, 13255 (2019).
- [62] F. Schindler, Z. Wang, M. G. Vergniory, A. M. Cook, A. Murani, S. Sengupta, A. Y. Kasumov, R. Deblock, S. Jeon, I. Drozdov, H. Bouchiat, S. Guron, A. Yazdani, B. A. Bernevig, and T. Neupert, Higher-order topology in bismuth, *Nat. Phys.* **14**, 918 (2018).
- [63] C. W. Peterson, W. A. Benalcazar, T. L. Hughes, and G. Bahl, A quantized microwave quadrupole insulator with topologically protected corner states, *Nature (London)* **555**, 346 (2018).
- [64] M. Serra-Garcia, V. Peri, R. Süsstrunk, O. R. Bilal, T. Larsen, L. G. Villanueva, and S. D. Huber, Observation of a phononic quadrupole topological insulator, *Nature (London)* **555**, 342 (2018).
- [65] Y. Xu, Z. Song, Z. Wang, H. Weng, and X. Dai, Higher-order topology of the axion insulator  $\text{EuIn}_2\text{As}_2$ , *Phys. Rev. Lett.* **122**, 256402 (2019).
- [66] S. Franca, J. van den Brink, and I. C. Fulga, An anomalous higher-order topological insulator, *Phys. Rev. B* **98**, 201114(R) (2018).
- [67] K. Kudo, T. Yoshida, and Y. Hatsugai, Higher-order topological Mott insulators, *Phys. Rev. Lett.* **123**, 196402 (2019).
- [68] R. Chen, C.-Z. Chen, J.-H. Gao, B. Zhou, and D.-H. Xu, Higher-order topological insulators in quasicrystals, *Phys. Rev. Lett.* **124**, 036803 (2020).

- [69] Y.-B. Yang, K. Li, L.-M. Duan, and Y. Xu, Higher-order topological Anderson insulators, *Phys. Rev. B* **103**, 085408 (2021).
- [70] Z. Yan, F. Song, and Z. Wang, Majorana corner modes in a high-temperature platform, *Phys. Rev. Lett.* **121**, 096803 (2018).
- [71] B. Y. Xie, G. X. Su, H. F. Wang, H. Su, X. P. Shen, P. Zhan, M. H. Lu, Z. L. Wang, and Y. F. Chen, Visualization of higher-order topological insulating phases in two-dimensional dielectric photonic crystals, *Phys. Rev. Lett.* **122**, 233903 (2019).
- [72] B. Zhu, Q. Wang, Y. Zeng, Q. J. Wang, and Y. D. Chong, Single-mode lasing based on  $\mathcal{PT}$ -breaking of two-dimensional photonic higher-order topological insulator, *Phys. Rev. B* **104**, L140306 (2021).
- [73] J. Zhu, W. Wu, J. Zhao, C. Chen, Q. Wang, X.-L. Sheng, L. Zhang, Y. X. Zhao, and S. A. Yang, Phononic real Chern insulator with protected corner modes in graphynes, *Phys. Rev. B* **105**, 085123 (2022).
- [74] F. F. Huang, P. Zhou, W. Q. Li, S. D. He, R. Tan, Z. S. Ma, and L. Z. Sun, Phononic second-order topological phase in the  $C_3N$  compound, *Phys. Rev. B* **107**, 134104 (2023).
- [75] M. Ezawa, Minimal models for Wannier-type higher-order topological insulators and phosphorene, *Phys. Rev. B* **98**, 045125 (2018).
- [76] M. J. Park, Y. Kim, G. Y. Cho, and S. B. Lee, Higher-order topological insulator in twisted bilayer graphene, *Phys. Rev. Lett.* **123**, 216803 (2019).
- [77] B. Liu, G. Zhao, Z. Liu, and Z. F. Wang, Two-Dimensional Quadrupole Topological insulator in  $\gamma$ -graphyne, *Nano Lett.* **19**, 6492 (2019).
- [78] E. Lee, R. Kim, J. Ahn, and B.-J. Yang, Two-dimensional higher-order topology in monolayer graphdiyne, *npj Quantum Mater.* **5**, 1 (2020).
- [79] X.-L. Sheng, C. Chen, H. Liu, Z. Chen, Z.-M. Yu, Y. X. Zhao, and S. A. Yang, Two-dimensional second-order topological insulator in graphdiyne, *Phys. Rev. Lett.* **123**, 256402 (2019).
- [80] Y. Ren, Z. Qiao, and Q. Niu, Engineering corner states from two-dimensional topological insulators, *Phys. Rev. Lett.* **124**, 166804 (2020).
- [81] X. Huang, J. Lu, Z. Yan, M. Yan, W. Deng, G. Chen, and Z. Liu, Acoustic higher-order topology derived from first-order with built-in Zeeman-like fields, *Sci. Bull.* **67**, 488 (2022).
- [82] Z.-Y. Zhuang and Z. Yan, Topological phase transitions and evolution of boundary states induced by Zeeman fields in second-order topological insulators, *Front. Phys.* **10**, 866347 (2022).
- [83] B. Han, J. Zeng, and Z. Qiao, In-Plane Magnetization-induced corner states in bismuthene, *Chin. Phys. Lett.* **39**, 017302 (2022).
- [84] C.-M. Miao, Q.-F. Sun, and Y.-T. Zhang, Second-order topological corner states in zigzag graphene nanoflake with different types of edge magnetic configurations, *Phys. Rev. B* **106**, 165422 (2022).
- [85] C.-M. Miao, Y.-H. Wan, Q.-F. Sun, and Y.-T. Zhang, Engineering topologically protected zero-dimensional interface end states in antiferromagnetic heterojunction graphene nanoflakes, *Phys. Rev. B* **108**, 075401 (2023).
- [86] C.-M. Miao, L. Liu, Y.-H. Wan, Q.-F. Sun, and Y.-T. Zhang, General principle behind magnetization-induced second-order topological corner states in the Kane-Mele model, *Phys. Rev. B* **109**, 205417 (2024).
- [87] C. Chen, Z. Song, J.-Z. Zhao, Z. Chen, Z.-M. Yu, X.-L. Sheng, and S. A. Yang, Universal approach to magnetic second-order topological insulator, *Phys. Rev. Lett.* **125**, 056402 (2020).
- [88] L. Liu, J. An, Y. Ren, Y.-T. Zhang, Z. Qiao, and Q. Niu, Engineering second-order topological insulators via coupling two first-order topological insulators, *Phys. Rev. B* **110**, 115427 (2024).
- [89] S.-Q. Shen, *Topological Insulators: Dirac Equation in Condensed Matter*, 2nd ed. (Springer, Berlin, 2017).